Wavefront sensing for aberration modeling in fluorescence MACROscopy

Praveen Pankajakshan[1], Alain Dieterlen[2], Zvi Kam[3], Gilbert Engler[4], Laure Blanc-Féraud[5], Josiane Zerubia[5], Jean-Christophe Olivo-Marin[1]

INSTITUT PASTEUR

ISBI 2011
March 31, 2011,
praveen@pasteur.fr

Road map

1. Fluorescence MACROscopy
2. Forward problem: Characterizing the aberration
3. Inverse problem: Wavefront sensing from intensity data
4. Take home message and ongoing work

Widefield fluorescence MACROscope

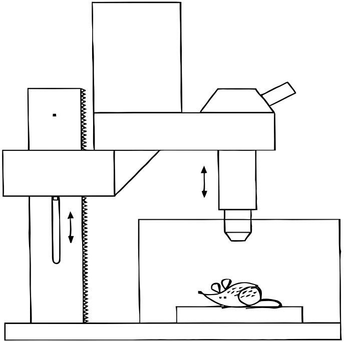

Widefield fluorescence MACROscope

Central points

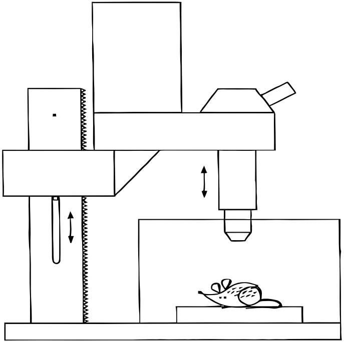

Widefield fluorescence MACROscope

Central points

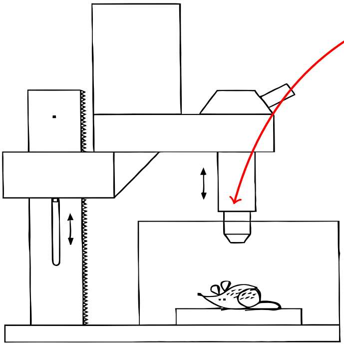

- Low magnification objective lens is combined with apochromatic zoom lens,

Widefield fluorescence MACROscope

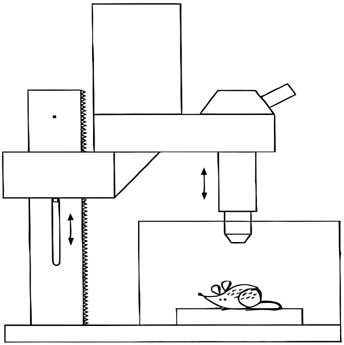

Central points

- Low magnification objective lens is combined with apochromatic zoom lens,
- permits large object fields (up to 35mm) and large working distances (up to 97mm),

Widefield fluorescence MACROscope

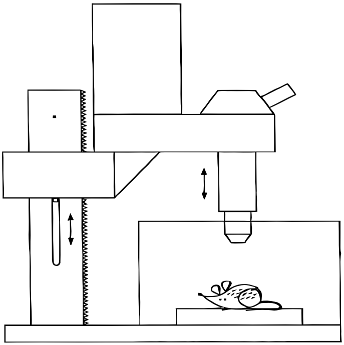

Central points

- Low magnification objective lens is combined with apochromatic zoom lens,
- permits large object fields (up to 35mm) and large working distances (up to 97mm),
- parallax-free and precise imaging,

Widefield fluorescence MACROscope

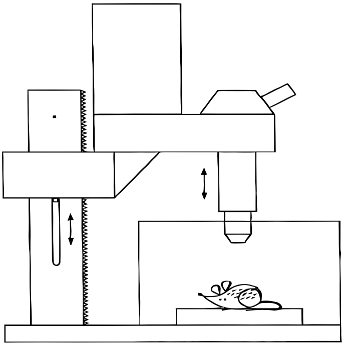

Central points

- Low magnification objective lens is combined with apochromatic zoom lens,
- permits large object fields (up to 35mm) and large working distances (up to 97mm),
- parallax-free and precise imaging,
- multi-color fluorescence.

Numerical aperture and resolution

$$\text{NA} \quad = \quad n_i \times \sin\alpha$$

Numerical aperture and resolution

$$\begin{aligned} \text{NA} &= n_i \times \sin\alpha \\ &= 1.00 \times \sin\alpha \end{aligned}$$

Numerical aperture and resolution

$$\begin{aligned} \text{NA} &= n_i \times \sin\alpha \\ &= 1.00 \times \sin\alpha \end{aligned}$$

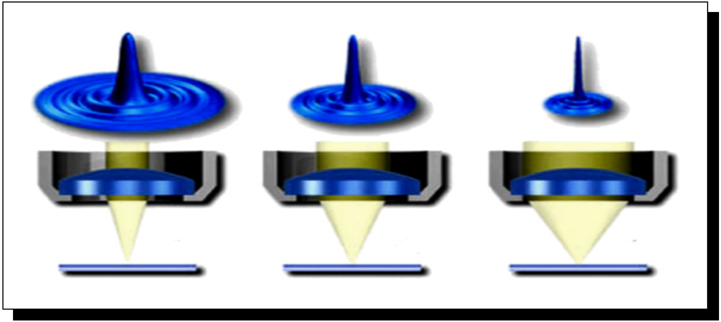

Numerical aperture and resolution

$$\text{NA} = n_i \times \sin\alpha$$
$$= 1.00 \times \sin\alpha$$

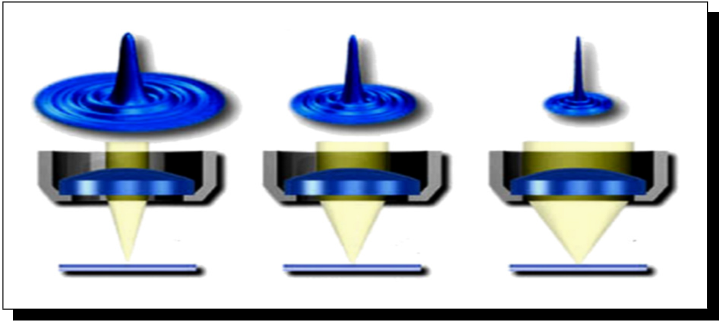

Numerical aperture decreases ←

Numerical aperture and resolution

$$\text{NA} = n_i \times \sin\alpha$$
$$= 1.00 \times \sin\alpha$$

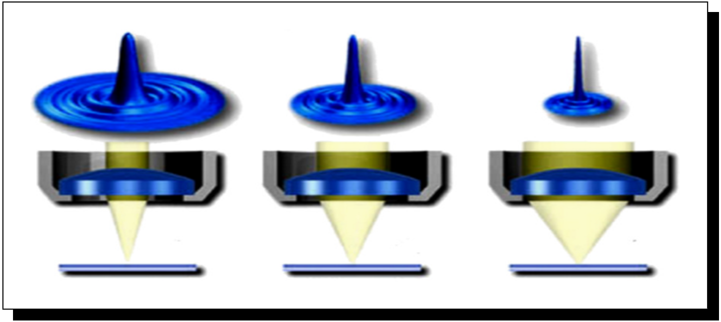

Numerical aperture decreases ←

Resolution decreases ←

Numerical aperture and working distance

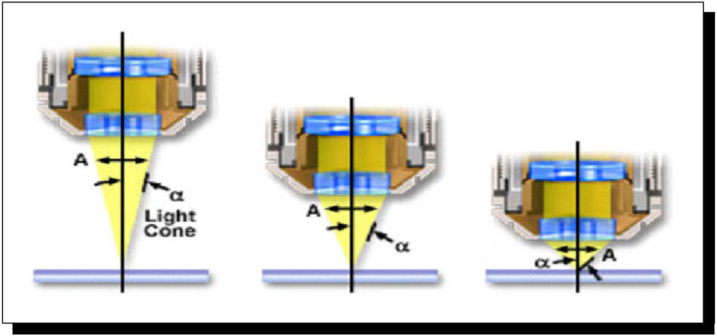

Numerical aperture and working distance

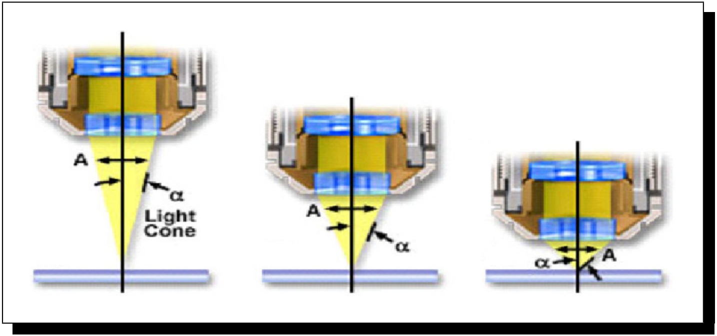

Numerical aperture increases

Numerical aperture and working distance

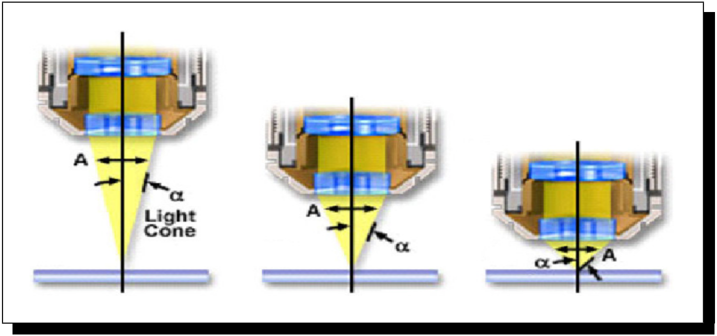

Numerical aperture increases →

Working distance & Field-of-view decreases →

Best of two worlds

Minimum zoom position

Best of two worlds

Maximum zoom position

Experimental impulse response

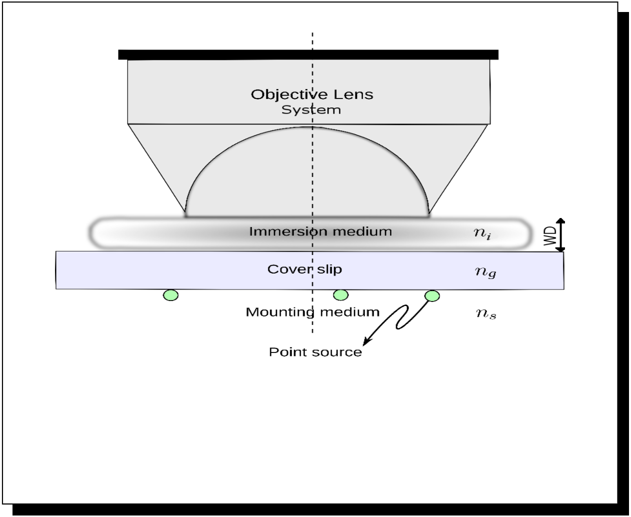

Experimental impulse response

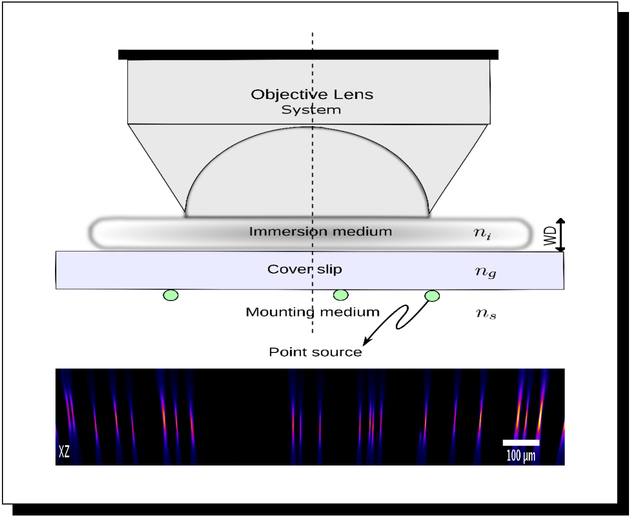

Figure 1: 2.5μm beads imaged using a Leica Widefield MacroFluo^{TM}Z16 APO fit with $5\times$ objective and the $1.6\times$ zoom. ©Herbomel lab, Pasteur Institute.

MACROscopes-Are they really the best of the two worlds?

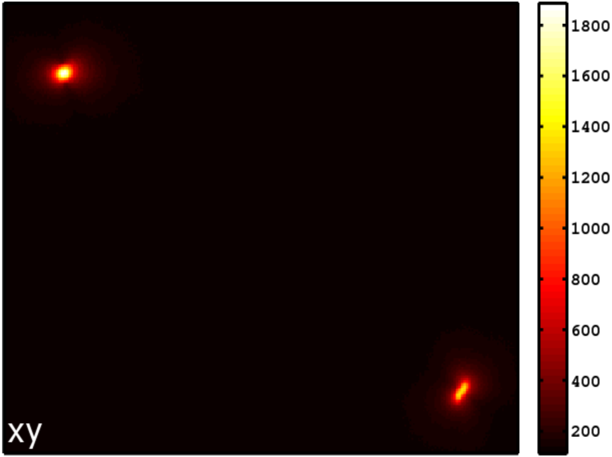

Figure 2: Axial projection of the beads. ©Herbomel lab, Pasteur Institute.

Forward problem: Characterizing the aberration

Incoherent scalar PSF model

- If $P(k_x, k_y, z)$ is the 2D complex pupil function and λ is the wavelength, the amplitude PSF can be calculated by just $2N_z$ number of 2D FFTs as

$$h_A(x, y, z; \lambda) = \int_{k_x} \int_{k_y} P(k_x, k_y, z) \exp(j(k_x x + k_y y))\, dk_y\, dk_x$$

Incoherent scalar PSF model

- If $P(k_x, k_y, z)$ is the 2D complex pupil function and λ is the wavelength, the amplitude PSF can be calculated by just $2N_z$ number of 2D FFTs as

$$h_A(x, y, z; \lambda) = \int_{k_x} \int_{k_y} P(k_x, k_y, z) \exp(j(k_x x + k_y y)) \, dk_y \, dk_x$$

- and the incoherent PSF is

$$h_{Th}(\mathbf{x}; \lambda_{\text{ex}}, \lambda_{\text{em}}) = C|h_A(\mathbf{x}; \lambda_{\text{ex}})| \times |h_A(\mathbf{x}; \lambda_{\text{em}})|$$

- λ_{ex} and λ_{em} are the excitation and emission peak wavelengths.

Limiting apertures overlapping

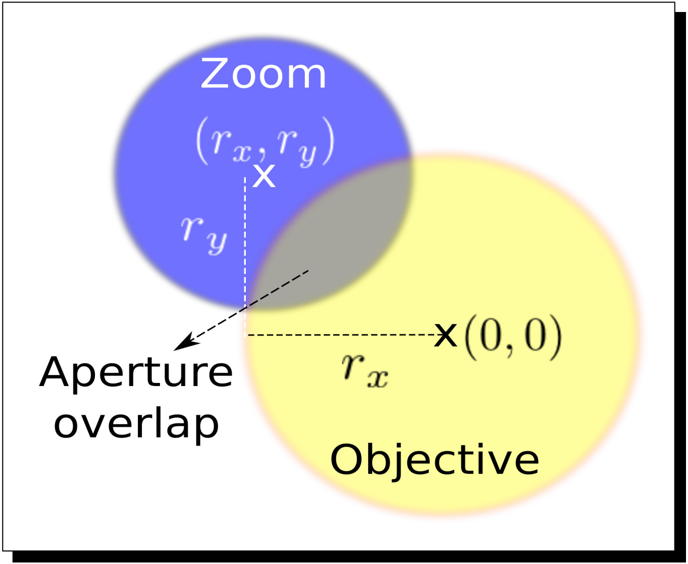

Limiting apertures overlapping

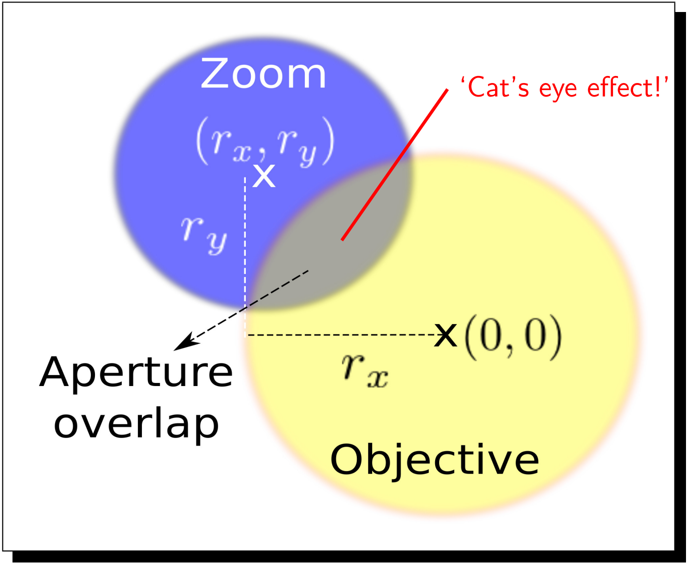

Optical vignetting

Figure 3: Lens viewed from the front. (Photograph by Peter Boehmer.)

Optical vignetting

Figure 3: Lens viewed from the front. (Photograph by Peter Boehmer.)

Figure 4: Lens viewed from the side. (Photograph by Peter Boehmer.)

PSF modeling by using scalar diffraction theory

- For a MICROscope, the pupil function is

PSF modeling by using scalar diffraction theory

- For a MICROscope, the pupil function is

$$P_m(k_x, k_y, z; \lambda) = \begin{cases} e^{jk_0\phi(\theta_i,\theta_s,z)}, & \text{if } \sqrt{k_x^2 + k_y^2} < \frac{2\pi}{\lambda}\mathsf{NA}_{\mathsf{Obj}} \\ 0, & \text{otherwise.} \end{cases}$$

PSF modeling by using scalar diffraction theory

- For a MICROscope, the pupil function is

$$P_m(k_x, k_y, z; \lambda) = \begin{cases} e^{jk_0\phi(\theta_i,\theta_s,z)}, & \text{if } \sqrt{k_x^2 + k_y^2} < \frac{2\pi}{\lambda}\mathsf{NA}_{\mathsf{Obj}} \\ 0, & \text{otherwise.} \end{cases}$$

- Modification for a MACROscope

$$P(k_x, k_y, z; \lambda) = \begin{cases} P_m, & \text{if } \sqrt{(k_x - r_x)^2 + (k_y - r_y)^2} < \frac{2\pi}{\lambda}\mathsf{NA}_{\mathsf{Zo}} \\ 0, & \text{otherwise.} \end{cases}$$

PSF modeling by using scalar diffraction theory

- For a MICROscope, the pupil function is

$$P_m(k_x, k_y, z; \lambda) = \begin{cases} e^{jk_0\phi(\theta_i,\theta_s,z)}, & \text{if } \sqrt{k_x^2 + k_y^2} < \frac{2\pi}{\lambda}\text{NA}_{\text{Obj}} \\ 0, & \text{otherwise.} \end{cases}$$

- Modification for a MACROscope

$$P(k_x, k_y, z; \lambda) = \begin{cases} P_m, & \text{if } \sqrt{(k_x - r_x)^2 + (k_y - r_y)^2} < \frac{2\pi}{\lambda}\text{NA}_{\text{Zo}} \\ 0, & \text{otherwise.} \end{cases}$$

- NA_{Obj} and NA_{Zo} are the objective and zoom lens NA; (r_x, r_y) are the relative displacements.

Characterization in the lateral field

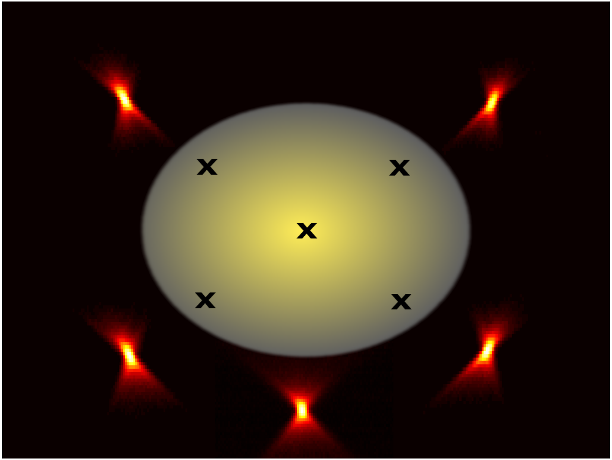

Figure 5: We can characterize the behavior at any position in the lateral field.

Out-of-focus highlights (OOFH)

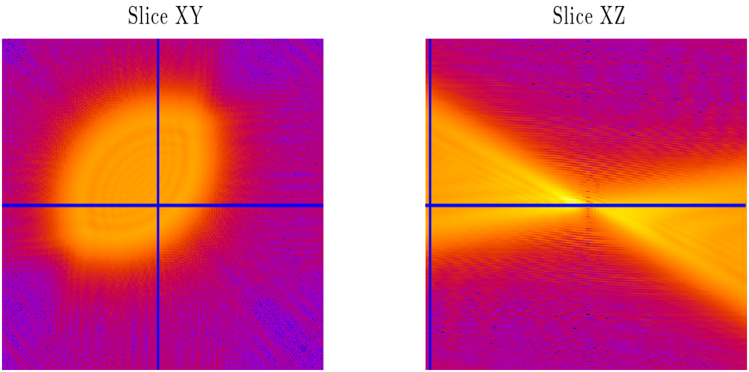

Figure 6: Theoretically calculated MACROscope PSF in log scale. NA$=0.5$, lateral sampling 178.33nm, axial sampling 1000nm.

Out-of-focus highlights (OOFH)

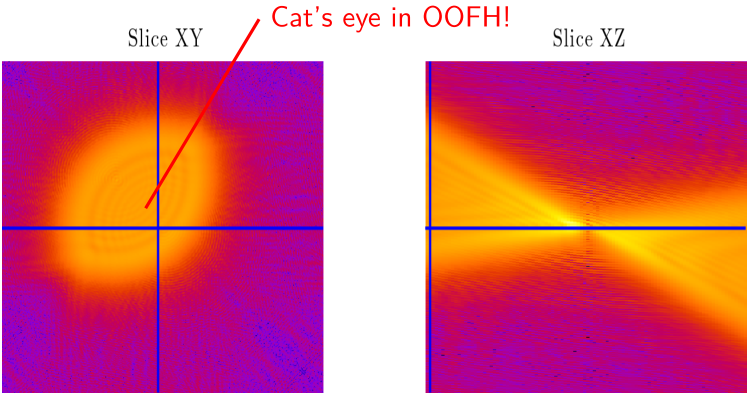

Figure 6: Theoretically calculated MACROscope PSF in log scale. NA$= 0.5$, lateral sampling 178.33nm, axial sampling 1000nm.

Inverse problem: Wavefront sensing from intensity data

Summary

Summary

- The PSF of an imaging system can vary experimentally,

Summary

- The PSF of an imaging system can vary experimentally,
- theoretically it can be calculated from the pupil function by a simple Fourier transform,

Summary

- The PSF of an imaging system can vary experimentally,
- theoretically it can be calculated from the pupil function by a simple Fourier transform,
- the pupil function is not often available,

Wavefront sensing from intensity data

Summary

- The PSF of an imaging system can vary experimentally,
- theoretically it can be calculated from the pupil function by a simple Fourier transform,
- the pupil function is not often available,
  - the wavefront can be sensed by using a Shack-Hartmann wavefront sensor,

Summary

- The PSF of an imaging system can vary experimentally,
- theoretically it can be calculated from the pupil function by a simple Fourier transform,
- the pupil function is not often available,
  - the wavefront can be sensed by using a Shack-Hartmann wavefront sensor,
  - it can be also retrieved from the observed intensities,

Wavefront sensing from intensity data

Summary

- The PSF of an imaging system can vary experimentally,
- theoretically it can be calculated from the pupil function by a simple Fourier transform,
- the pupil function is not often available,
  - the wavefront can be sensed by using a Shack-Hartmann wavefront sensor,
  - it can be also retrieved from the observed intensities,
- the aberrations in the optics of the objective can be determined by studying this phase,

Summary

- The PSF of an imaging system can vary experimentally,
- theoretically it can be calculated from the pupil function by a simple Fourier transform,
- the pupil function is not often available,
  - the wavefront can be sensed by using a Shack-Hartmann wavefront sensor,
  - it can be also retrieved from the observed intensities,
- the aberrations in the optics of the objective can be determined by studying this phase,
- the estimated wavefront can be used to correct the aberrated optical path.

Wavefront sensing-a Bayesian interpretation

- For uncorrelated low photon count data the observation is:

$$i(\mathbf{x}) = \mathcal{P}\{|h_{\mathsf{A}}(\mathbf{x})|^2 + b(\mathbf{x})\}, \forall \mathbf{x} \in \Omega_s$$

Wavefront sensing-a Bayesian interpretation

- For uncorrelated low photon count data the observation is:

$$i(\mathbf{x}) = \mathcal{P}\{|h_{\mathsf{A}}(\mathbf{x})|^2 + b(\mathbf{x})\}, \forall \mathbf{x} \in \Omega_s$$

- Considering Poissonian photon counting statistics, the likelihood of obtaining image $i(x)$ from a diffraction-limited point source:

$$\Pr(i|h_{\mathsf{A}}) = \prod_{\mathbf{x}\in\Omega_s} \frac{(h_{\mathsf{A}} + b)(\mathbf{x})^{i(\mathbf{x})} \exp(-(h_{\mathsf{A}} + b)(\mathbf{x}))}{i(\mathbf{x})!}$$

Wavefront sensing-a Bayesian interpretation

- For uncorrelated low photon count data the observation is:

$$i(\mathbf{x}) = \mathcal{P}\{|h_\mathsf{A}(\mathbf{x})|^2 + b(\mathbf{x})\}, \forall \mathbf{x} \in \Omega_s$$

- Considering Poissonian photon counting statistics, the likelihood of obtaining image $i(x)$ from a diffraction-limited point source:

$$\Pr(i|h_\mathsf{A}) = \prod_{\mathbf{x}\in\Omega_s} \frac{(h_\mathsf{A}+b)(\mathbf{x})^{i(\mathbf{x})}\exp(-(h_\mathsf{A}+b)(\mathbf{x}))}{i(\mathbf{x})!}$$

- From the Bayes' theorem, the *a posteriori* is

$$\Pr(h_\mathsf{A}|i) = \frac{\Pr(i|h_\mathsf{A})\Pr(h_\mathsf{A})}{\Pr(i)}$$

Global idea for sensing

- Invariant to defocus

Global idea for sensing

- Invariant to defocus

$$P(k_x, k_y, z) = \begin{cases} e^{jk_0(\varphi_{\text{aberr}} + \phi_{\text{defocus}}(\theta_i, z))}, & \text{if } \sqrt{k_x^2 + k_y^2} < \frac{2\pi}{\lambda}\text{NA} \\ 0, & \text{otherwise.} \end{cases}$$

Global idea for sensing

- Invariant to defocus

$$P(k_x, k_y, z) = \begin{cases} e^{jk_0(\varphi_{\text{aberr}} + \phi_{\text{defocus}}(\theta_i, z))}, & \text{if } \sqrt{k_x^2 + k_y^2} < \frac{2\pi}{\lambda}\text{NA} \\ 0, & \text{otherwise.} \end{cases}$$

- Estimate the near-focus amplitude distribution, $\hat{h}_{\text{A}}$, by maximizing the *a posteriori* (MAP) or minimizing the cologarithm of the *a posteriori*

$$\hat{h}_{\text{A}}(\mathbf{x}; \varphi_{\text{aberr}}) = \arg\min_{h_{\text{A}}(\mathbf{x})} -\log[\Pr(h_{\text{A}}|i)], \text{s. t. } k_{\text{MAX}} < \frac{2\pi\text{NA}}{\lambda_{\text{ex}}}$$

k_{MAX} is the pupil support,

- this can be solved by using a fixed-point iterative algorithm.

Experiment on intensity data

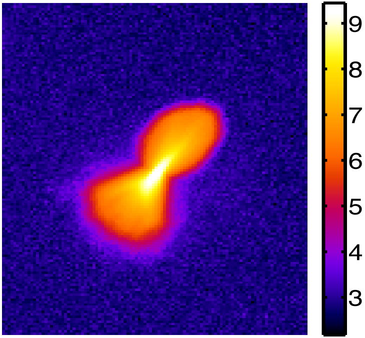

Figure 7: Radially projected 2.5μm observed intensity volume. ©Imaging Center, IGBMC, France.

Experiment on intensity data

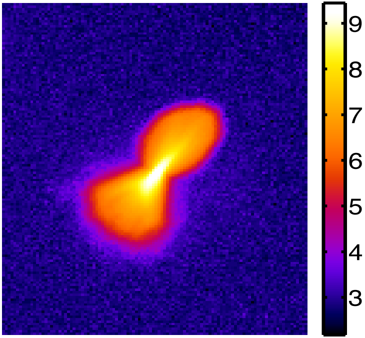

Figure 7: Radially projected 2.5μm observed intensity volume. ©Imaging Center, IGBMC, France.

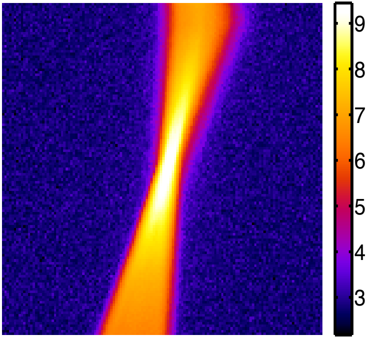

Figure 8: Axially projected 2.5μm observed intensity volume. ©Imaging Center, IGBMC, France.

Experiment on intensity data

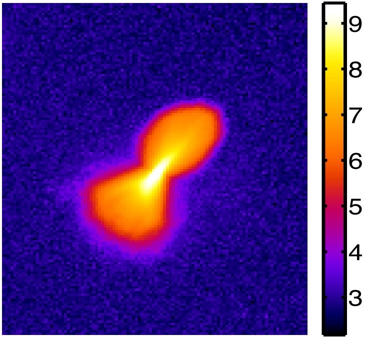

Figure 7: Radially projected 2.5μm observed intensity volume. ©Imaging Center, IGBMC, France.

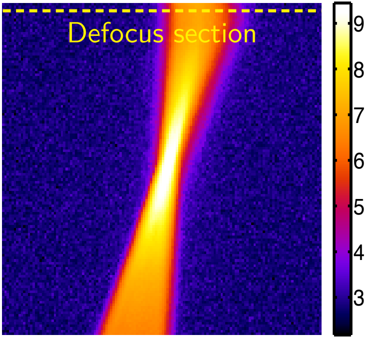

Figure 8: Axially projected 2.5μm observed intensity volume. ©Imaging Center, IGBMC, France.

Wavefront sensed from intensity data

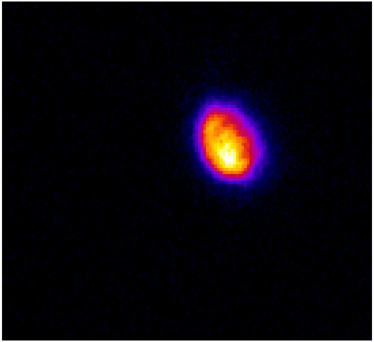

Figure 9: OOFH radial section of the observed volume, z $= -57\mu$m. ©Imaging Center, IGBMC, France.

Costantini, M. (1998). A novel phase unwrapping method based on network programming. IEEE Tran. on Geoscience and Remote Sensing, 36, 813-821.

Wavefront sensed from intensity data

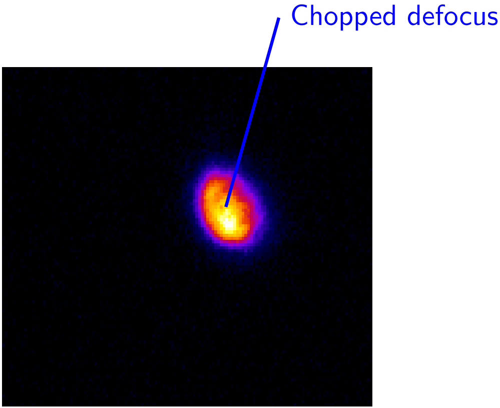

Figure 9: OOFH radial section of the observed volume, z $= -57\mu$m.

Costantini, M. (1998). A novel phase unwrapping method based on network programming. IEEE Tran. on Geoscience and Remote Sensing, 36, 813-821.

Wavefront sensed from intensity data

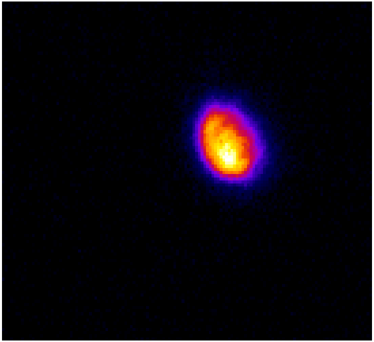

Figure 9: OOFH radial section of the observed volume, z $= -57\mu$m. ©Imaging Center, IGBMC, France.

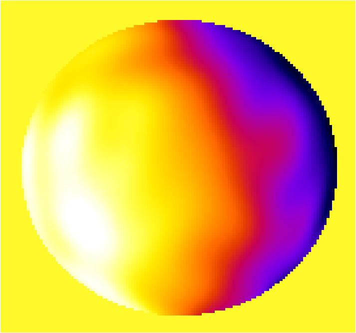

Figure 10: Retrieved unwrapped pupil phase from the intensity images $\tau = 0.9$ and the maximum number of iteration is 40.

Costantini, M. (1998). A novel phase unwrapping method based on network programming. IEEE Tran. on Geoscience and Remote Sensing, 36, 813-821.

Wavefront sensed from intensity data

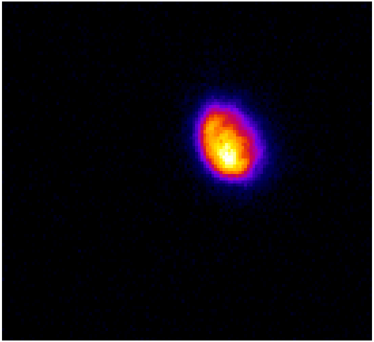

Figure 9: OOFH radial section of the observed volume, z $= -57\mu$m. ©Imaging Center, IGBMC, France.

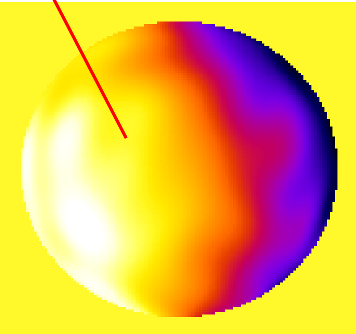

Figure 10: Retrieved unwrapped pupil phase from the intensity images $\tau = 0.9$ and the maximum number of iteration is 40.

Costantini, M. (1998). A novel phase unwrapping method based on network programming. IEEE Tran. on Geoscience and Remote Sensing, 36, 813-821.

Take home message

- The MACROscope PSF varies as a function of the lateral field position,

Take home message

- The MACROscope PSF varies as a function of the lateral field position,
- vignetting was observable only for smaller zooms (large FOV) and is negligible for larger zooms,

Take home message

- The MACROscope PSF varies as a function of the lateral field position,
- vignetting was observable only for smaller zooms (large FOV) and is negligible for larger zooms,
- exploit defocus sections phase aberration invariancy to estimate the back focal plane pupil phase,

Take home message

- The MACROscope PSF varies as a function of the lateral field position,
- vignetting was observable only for smaller zooms (large FOV) and is negligible for larger zooms,
- exploit defocus sections phase aberration invariancy to estimate the back focal plane pupil phase,
- the wavefront estimated from the experimental bead intensity data validates the vignetting hypothesis,

Take home message

- The MACROscope PSF varies as a function of the lateral field position,
- vignetting was observable only for smaller zooms (large FOV) and is negligible for larger zooms,
- exploit defocus sections phase aberration invariancy to estimate the back focal plane pupil phase,
- the wavefront estimated from the experimental bead intensity data validates the vignetting hypothesis,
- the sensed wavefront can be used to define the effective working zoom,

Take home message

- The MACROscope PSF varies as a function of the lateral field position,
- vignetting was observable only for smaller zooms (large FOV) and is negligible for larger zooms,
- exploit defocus sections phase aberration invariancy to estimate the back focal plane pupil phase,
- the wavefront estimated from the experimental bead intensity data validates the vignetting hypothesis,
- the sensed wavefront can be used to define the effective working zoom,
- ongoing work: restore the images by correcting for the field aberration and also the diffraction effects.

Acknowledgements

- The first author wish to thank ANR DIAMOND for funding the postdoctoral research fellowship,

Acknowledgements

- The first author wish to thank ANR DIAMOND for funding the postdoctoral research fellowship,
- the authors are grateful to Dr. Philippe Herbomel from the Institut Pasteur, France and Dr. Didier Hentsch from IGBMC, France for the images and the discussions,

Acknowledgements

- The first author wish to thank ANR DIAMOND for funding the postdoctoral research fellowship,
- the authors are grateful to Dr. Philippe Herbomel from the Institut Pasteur, France and Dr. Didier Hentsch from IGBMC, France for the images and the discussions,
- some of the bead samples were prepared by Dr. Mickael Lelek from Institut Pasteur, France, a big thanks to him,

INSTITUT PASTEUR

Acknowledgements

- The first author wish to thank ANR DIAMOND for funding the postdoctoral research fellowship,
- the authors are grateful to Dr. Philippe Herbomel from the Institut Pasteur, France and Dr. Didier Hentsch from IGBMC, France for the images and the discussions,
- some of the bead samples were prepared by Dr. Mickael Lelek from Institut Pasteur, France, a big thanks to him,
- we acknowledge our colleagues for their support.

Acknowledgements

- The first author wish to thank ANR DIAMOND for funding the postdoctoral research fellowship,
- the authors are grateful to Dr. Philippe Herbomel from the Institut Pasteur, France and Dr. Didier Hentsch from IGBMC, France for the images and the discussions,
- some of the bead samples were prepared by Dr. Mickael Lelek from Institut Pasteur, France, a big thanks to him,
- we acknowledge our colleagues for their support.

For more information see:
http://www-syscom.univ-mlv.fr/ANRDIAMOND/

Acknowledgements

- The first author wish to thank ANR DIAMOND for funding the postdoctoral research fellowship,
- the authors are grateful to Dr. Philippe Herbomel from the Institut Pasteur, France and Dr. Didier Hentsch from IGBMC, France for the images and the discussions,
- some of the bead samples were prepared by Dr. Mickael Lelek from Institut Pasteur, France, a big thanks to him,
- we acknowledge our colleagues for their support.

For more information see:
http://www-syscom.univ-mlv.fr/ANRDIAMOND/

Thank you!